Hindawi
International Journal of Antennas and Propagation
Volume 2019, Article ID 6098483, 8 pages
https://doi.org/10.1155/2019/6098483

Research Article

Low-RCS, Circular Polarization, and High-Gain Broadband Antenna Based on Mirror Polarization Conversion Metasurfaces

Liang Zhang,[1,2] **Changqing Liu**,[1] **Chun Ni**,[2] **Meng Kong**,[2] **and Xianliang Wu**[1]

[1]*Key Lab of Intelligent Computing & Signal Processing, Ministry of Education, Anhui University, Hefei 230601, China*
[2]*Key Laboratory of Simulation and Design for Electronic Information System of Anhui Province, Hefei 230601, China*

Correspondence should be addressed to Liang Zhang; liangzh@hfnu.edu.cn

Received 22 February 2019; Revised 28 June 2019; Accepted 24 July 2019; Published 6 August 2019

Guest Editor: Massimo Donelli

In this paper, a novel slot antenna array that is based on mirror polarization conversion metasurfaces (MPCM) is proposed. It achieves circular polarization (CP) and effectively reduces the radar cross section (RCS) and increases gain in the entire x-band. This design uses the mirrored composition of the polarization conversion metasurfaces (PCM) on the top surface of the substrate. The MPCM covers a 2×2 slot antenna array that is fed with by a sequentially rotating network. The CP radiation is realized by the polarization conversion characteristics of the PCM. At the same time, the reduction of RCS is achieved by 180° ($\pm 30^{\circ}$) reflection phase difference between two adjacent PCMs. The improvement in gain is achieved by using a Fabry–Perot cavity, which is constituted by the ground of the antenna and the PCM. Simulated and measured results show that approximately 46.4% of the operating bandwidth is in the range of 7.5–12 GHz (AR < 3 dB) and the gain of the antenna with MPCM is at least 5 dB higher than the reference antenna. Moreover, the monostatic RCS is reduced from 8 to 20 GHz.

1. Introduction

With the rapid development of modern radio technology, great breakthroughs have been made in wireless communication systems, radar navigation, carrier stealth, and other related fields. A multifunction antenna based on electromagnetic metasurfaces can adequately satisfy the requirements of complex systems and concurrent tasks. Therefore, developing a high-gain antenna with a low radar cross section (RCS) that produces circular polarization (CP) is an important subject among experts and scientists [1–8].

A metasurface (MS) is a two-dimensional metamaterial structure with a low profile, low loss, and a simple design. MS has many significant advantages in polarization control, and it has been used in low-RCS antenna as well as RCS reduction design [6–14]. Recently, Akgol et al. proposed a metasurface that uses a polarization converter to convert linear polarization signals to circular polarization signals while having a 3 dB axial ratio bandwidth of 800 MHz [3–5]. In [6–8], the idea of using a partial reflector to achieve a low RCS and high gain was proposed. By adding a resistor to the structure, the energy of the incoming electromagnetic wave can be absorbed to reduce the backward RCS. However, due to the need to weld a large number of resistors, it is difficult to manufacture the antenna in practice. In [10], a new metamaterial surface antenna based on the chessboard polarization conversion metasurface (CPCM) was proposed. Using this approach, a broadband antenna with low RCS, CP, and high gain could be realized by placing a 12 mm MS above the feed antenna. However, the antenna requires a large volume and the axial ratio (AR) bandwidth is narrow. In [11], an MS-based antenna array was proposed, which could realize both circular polarization and RCS reduction, providing a good method for RCS reduction; however, the antenna structure is complex and the impedance bandwidth is narrow. Although the method proposed above has made significant progress, the application of MS experiences considerable shortcomings. In the state-of-the-art designs, low-profile antennas that simultaneously achieve wideband RCS reduction and wideband CP remain a challenge.

To further realize the integration of multiple performances on one antenna, this paper proposes a broadband low-RCS, low-profile CP, high-gain antenna based on mirror supersurface. The AR bandwidth is expanded by means of sequential

rotation feeding [15, 16]. Circular polarization, RCS reduction, and gain enhancement can be realized in the entire x-band. The antenna array achieves a larger RCS reduction and AR bandwidth than the CP slot antenna that is described in published literature. Compared with the low-RCS Fabry–Perot resonant cavity that is based on MS, the proposed antenna has an important advantage. It is low profile and without air gap, which means that it can be applied in many fields.

2. Design of the Mirror Polarization Conversion Metamaterials

2.1. Structure of the Antenna. Figures 1(a)–1(c) illustrate the structure of the antenna, which is composed of an MPCM and a slot antenna array (as the source antenna). The MPMS consists of four parts: Part I is an MPCM, parts II and IV are its mirror images, and part III is the mirror image of part II. Figure 2(a) shows an enlarged view of the PCM with a linear polarization (LP) slot antenna source. The PCM is composed of 4×4 square cells with different corners truncated on both sides. In order to expand the AR bandwidth, the feed antenna is supplied data from the network as it rotates in sequence. The phase distribution is 0°, 90°, 180°, and 270°, as shown in Figure 1(c). The substrate utilized is Rogers RO4003C with $\varepsilon_r = 3.55$ and a loss tangent of $\delta = 0.0027$. The optimized widths are as follows: $w1 = 0.18$ mm, $w2 = 0.47$ mm, $w3 = 0.16$ mm, $w4 = 0.31$ mm, $w5 = 0.47$ mm, $w6 = 0.13$ mm, $w7 = 0.47$ mm, $w8 = 0.9$ mm, and $wf = 1.13$ mm and $r = 3.5$ mm.

Each PCM performs three functions. First, when an LP wave passes through the PCM, it is converted into CP wave. Second, the PCM can achieve reflective wave wideband polarization conversion. Third, an increase in the gain is realized by the Fabry–Perot cavity that is formed by the slot array antenna and the PCM. Obviously, it is very difficult to adjust these three functions at the same time. Therefore, the objective of this research is to balance these features. The general procedure for the design of the PCM can be summarized as follows:

(1) The unit cell PCM, covering the operation band (8–12 GHz) of the antenna, is designed to obtain the initial parameters

(2) The copolarization and cross-polarization transmission coefficients are modified by optimizing the diagonal corner truncated on both sides of the unit cell. This will convert the LP wave into the CP wave

(3) Optimize the x-component and y-component of the reflection coefficient to meet the Fabry–Perot resonance condition of CP

(4) Optimize the polarization conversion unit cell with flooring (Figure 3) to realize broadband polarization conversion

(5) Repeat steps 2–4 until the process is complete

Following the design steps above, the final parameters of the unit cell are as follows: $a = 4.6$ mm, $d1 = 1.2$ mm, $d2 = 2.8$ mm, $c = 0.4$ mm, $b = 25$ mm, $Ws = 2.2$, $Ls = 14.4$ mm, $L1 = 3.9$ mm, $h0 = 0.508$ mm, and $h1 = 2$ mm.

2.2. Analysis of the Circular Polarization. One way to describe an array antenna is that it consists of four PCM-based CP antennas, which are arranged in 90° rotations. An equivalent circuit can be used to explain the formation of CP. In Figure 2(a), the structure within the area enclosed by the red square can be considered a new unit. When the PCM is placed on the slot antenna, which is LP along the y-axis, an E-field is generated along the y-axis. The E-field is broken down into orthogonal components $\vec{E}_1$ and $\vec{E}_2$, as shown in Figure 2(c). If the diagonal of the unit is not truncated, due to the symmetry of the structure, as shown in Figure 2(b), the orthogonal components $\vec{E}_1$ and $\vec{E}_2$ constitute an RLC circuit with an impedance given by [17]

$$Z = 2R + j\omega(2L) + \frac{1}{j\omega C} = R' + jX', \tag{1}$$

where L and R are the inductance and resistance of the patch and C is the capacitance generated by the gap between nearby and related units. When the diagonal corners are truncated as shown in Figure 2(c), the perpendicular E-field components that are broken down by the PCM will cause two different impedances, $Z_1$and Z_2. The expression for the two impedances is shown in the following equations:

$$Z_1 = R_1' + jX_1', \tag{2}$$

$$Z_2 = R_2' + jX_2'. \tag{3}$$

The truncation corner increases the gaps between nearby and related patches, thereby increasing the value of X_1' and decreasing the value of X_2'. Thus, the phase difference between Z_1 and Z_2 can be changed by modifying the value of the truncated corners on both sides. If the PCM is designed such that $|Z_1| = |Z_1|$ and $\angle Z_2 - \angle Z_1 = 90°$, then $|\vec{E}_1| = |\vec{E}_2|$ and $\angle \vec{E}_2 - \angle \vec{E}_1 = 90°$.

Figure 4(a) presents a comparison of the reflection coefficients for slot antennas both with and without PCM. As shown in Figure 4(b), the axial ratio (AR < 3 dB) bandwidth of the slot antenna with PCM ranges from 9.2 to 10 GHz. The results show that PCM can have the ability to transform the LP wave into a CP wave. In addition, the gain has been improved. The reasons for this improvement are explained in the following section.

2.3. Mechanism of High-Gain Performance. A metamaterial surface (MS) is essentially the surface distribution of a small electrical scatterer [18]. Due to its planar structure, it can be easily combined with a planar antenna to form a resonant cavity. As shown in Figure 2(a), when the spacing between the reflective floor and the MS meets the resonance condition, the electromagnetic wave is constantly reflected back and forth in the resonant cavity. Also, the electromagnetic wave transmitted through the MS can be superimposed with the phase each time. Thus, the gain and beam width of the antenna are improved, and the radiation energy can be directed by adjusting the height between the two plates. According to the analysis in the literature [19], two resonant modes (TM_{10} mode and antiphase TM_{20} mode) are simultaneously excited to load the metamaterial

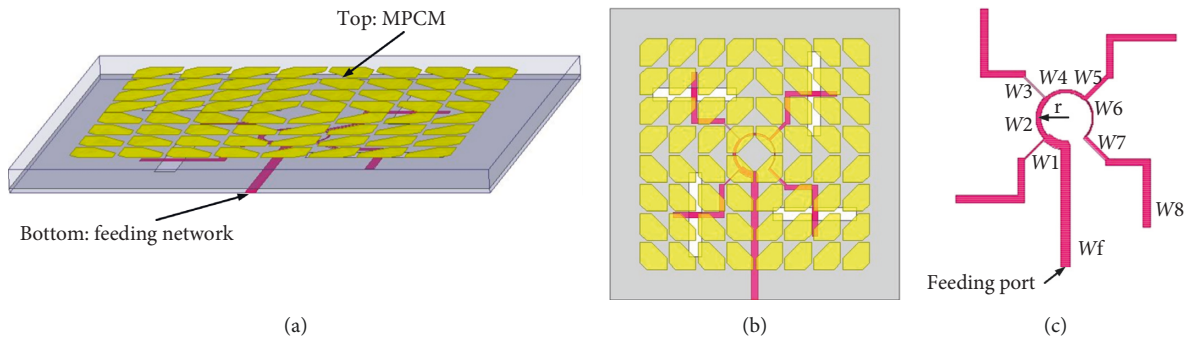

Figure 1: (a) The schematic view of the array. (b) The top view of the array. (c) The feeding network.

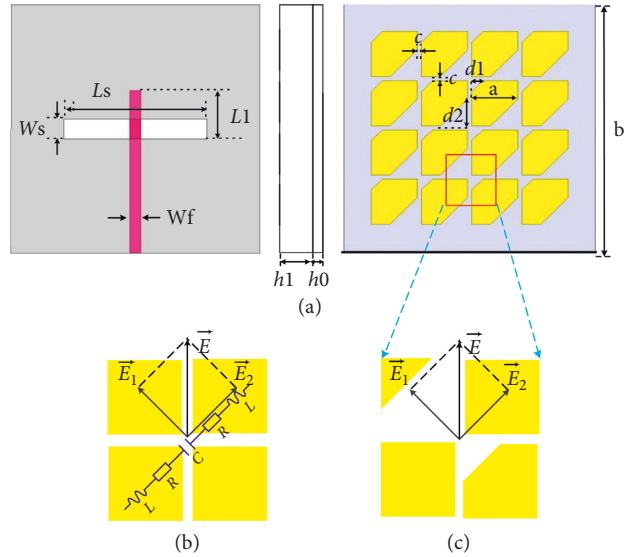

Figure 2: (a) CP antenna. (b) New unit cell without truncation. (c) New unit cell with diagonal.

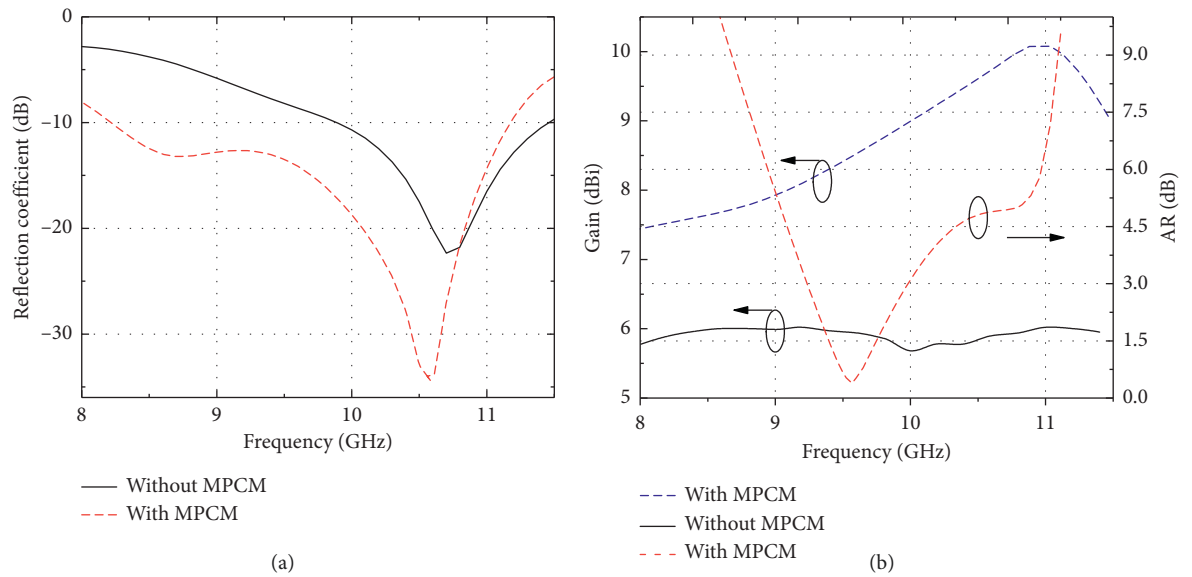

Figure 3: Simulated (a) reflection coefficients and (b) boresight gain and AR versus frequency of the slot antenna with and without PCM.

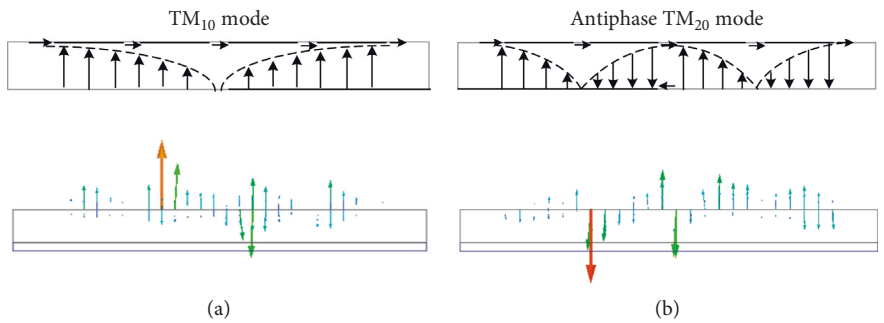

Figure 4: Two resonant modes of the proposed antenna. (a) 8.6 GHz and (b) 10.5 GHz.

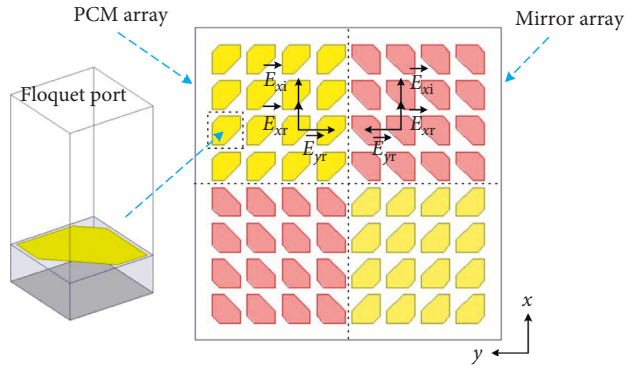

Figure 5: The PCM unit cell and top view of a mirror composed of four parts.

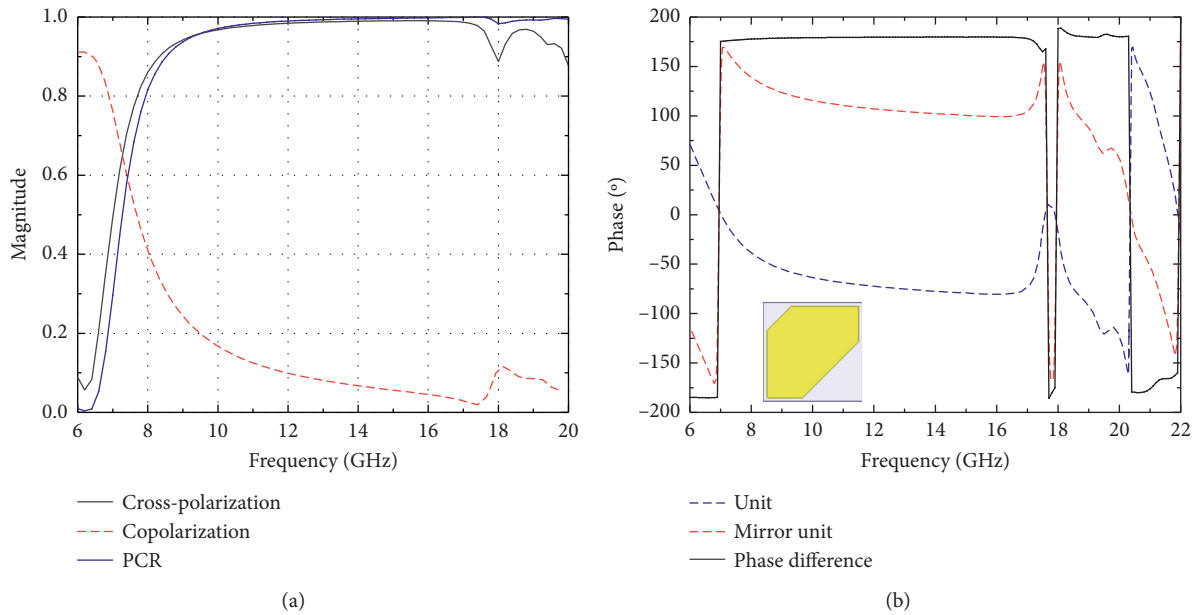

Figure 6: (a) Reflection coefficients of copolarization, cross-polarization, and PCR. (b) The cross-polarized reflection phase difference between the infinite periodic unit cell and its mirror.

element of the slot antenna. This in turn leads to the low-profile wideband LP antenna. Due to the distribution of the truncated diagonal corner, the impedance matching bandwidth is improved. However, the gain is less affected. Figures 5(a) and 5(b) show the electric field distribution at two distinct frequencies (8.6 and 10.5 GHz), verifying its two resonant modes: TM_{10} mode and TM_{20} inversion mode.

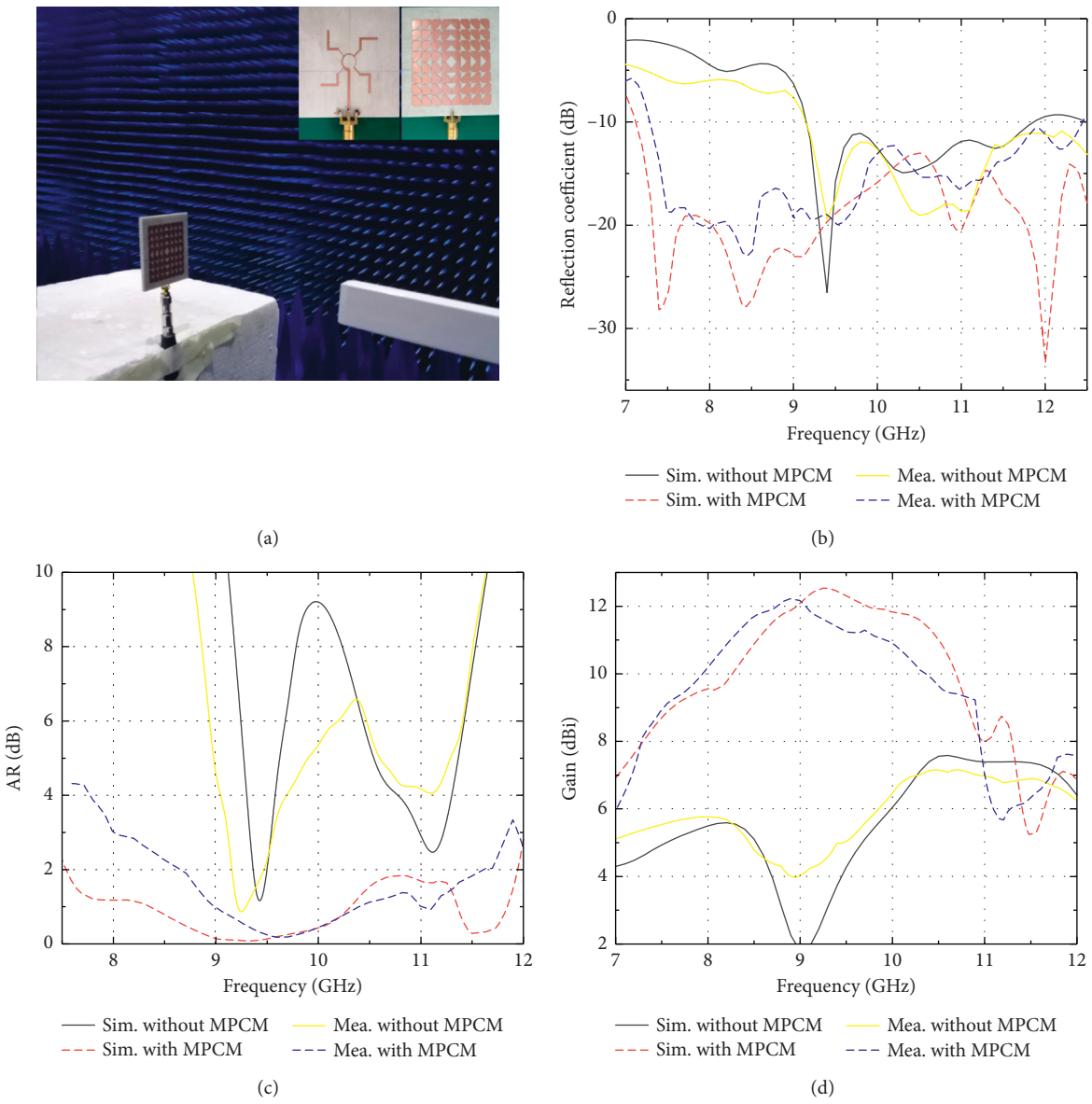

Figure 7: (a) The photograph of fabricated and measured. Simulated and measured (b) reflection coefficients, (c) AR, and (d) gain versus frequency of both antennas.

2.4. Analysis of RCS Reduction. As shown in Figure 3, the MPCM patch can be regarded as a checkerboard surface that consists of a PCM array and mirror PCM array. A phase difference of 180° is created between each part, so that the reflected waves for each will cancel each other out. Consequently, the total RCS is significantly reduced. In order to study the RCS reduction characteristics of the array antenna, the polarization conversion characteristics of the PCM element need to be studied. When the incident wave impinges along the z-direction, the unit cell can be considered a reflective polarization converter. As shown in Figure 3, using the linear x-polarized normal-impinging wave $\vec{E}^{\mathrm{i}}_x$ as an example, the reflected electric fields $\vec{E}^{\mathrm{r}}_x$ and $\vec{E}^{\mathrm{r}}_y$ along the x-axis and the y-axis are generated. Definitions $r_{xx} = |\vec{E}^{\mathrm{r}}_x / \vec{E}^{\mathrm{i}}_x|$ (copolarization) and $r_{yx} = |\vec{E}^{\mathrm{r}}_y / \vec{E}^{\mathrm{i}}_x|$ (cross-polarization) represent the reflection ratio in the x-x and x-y directions, respectively. The polarization conversion ratio (PCR) is defined as PCR $= r^2_{yx} / (r^2_{yx} + r^2_{xx})$, representing the polarization conversion characteristics for the PCM cell. The PCM unit cell has been simulated in the software Ansys HFSS v13.0, using the Floquet port and master/slave boundary conditions. The results presented in Figure 6(a) show that the copolarization of the reflection coefficient loses its dominant position within 8–20 GHz, whereas the cross-polarization becomes the dominant component. The PCR value is greater than 0.7 between 8 and 20 GHz, which means that most of the energy is redirected in the orthogonal direction. Figure 6(b) presents the cross-polarization reflection phase difference between the PCM infinite period unit and its mirror. In the working frequency band, the reflected wave of PCM has the same amplitude as that of the corresponding

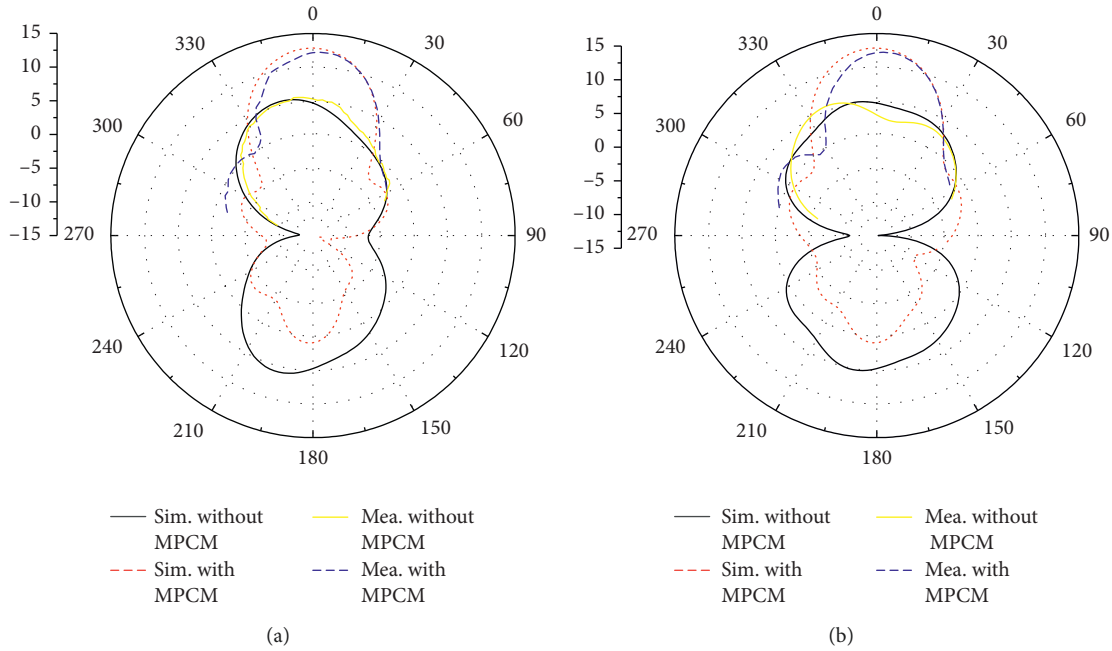

Figure 8: The simulated normalized radiation pattern of both antennas at 10 GHz. (a) *xoz*-plane and (b) *yoz*-plane.

mirror image, with a phase difference of 180°. The reflected waves from each part cancel each other out, decreasing the RCS. Due to the symmetrical structure of the MPCM, the reduction in RCS of the y-polarized incident wave is similar. As a result, the mirror chessboard PCM structure is chosen due to its broadband, low-RCS features.

Considering the arrangement of MPCM, the corresponding slot antennas under each PCM should not be configured such that they are in the same direction, and they should not be excited by the same phase. Therefore, a CP slot array antenna based on a sequential rotational feed network is selected as the source antenna. Because the reference antenna also utilizes circular polarization radiation, it may seem unnecessary to use MPCM for the same purpose. However, antennas using MPCM have a wider AR bandwidth because a superior polarization purity can be obtained by replacing four LP components with four CP components. In addition, gain can be increased at operating frequencies, so the radiation performance and scattering characteristics are balanced by the combination of the arrangement of the MPCM and the radiation source.

3. Simulation and Measurement Comparison of Both Antennas

In order to verify the correctness of simulation and analysis, an array sample with a size of $50 \times 50 \times 2.5\ \text{mm}^2$ was created and measured. The spacing of each slot is 20.7 mm, approximately 0.6 λ_0 (relative to the operating frequency of 10 GHz). The radiation patterns of the antenna are measured in a microwave chamber without reflection, as shown in Figure 7(a). The reflection coefficient of the antenna was measured using an Agilent N5247A vector network analyzer.

Figure 7(b) shows the reflection coefficient results, both with and without the MCPM antenna simulation and measurement. Although there exists some deviation, the overall results are consistent. The measurement and simulation AR bandwidth for the two antennas are shown in Figure 7(c). The measured CP operating bandwidth is 8–12 GHz (40%), whereas the simulated CP operating bandwidth is 7.5–12 GHz (46.1%). The results indicate that the AR bandwidth can be extended by using the MPCM. Figure 7(d) shows the gain versus frequency plot for the simulation and measurement of the antenna. The gain of an antenna with MPCM is higher from 7–11.2 GHz, compared to that of an antenna without MPCM. The measured 3 db gain is in the 7.7–10.5 GHz band (30.7%), whereas the simulated one is in the 7.9–10.8 GHz band (31%). The main cause for the offset in frequency is attributed to both manufacturing error and error in measurement. Figures 8(a) and 8(b) depict the measurement and simulation patterns of the two antennas at 9.3 GHz. The difference between simulation and measurement is due to the measurement environment, manufacturing tolerances, and assembly errors. The test and simulation results in Figures 7 and 8 show good consistency overall, verifying that the use of MPCM improves the radiation performance.

The 3D bistatic scattering field at 10 GHz under normal incidence, both with and without the MPCM antenna, is shown in Figures 9(b) and 9(c). The normal directional energy of the scattered wave is redistributed in four directions $(\varphi, \theta) = (45^\circ, 46^\circ)$, $(135^\circ, 46^\circ)$, $(225^\circ, 46^\circ)$, and $(315^\circ, 46^\circ)$. The frequency response of the measured and simulated monostatic RCS in the x-polarized normal-impinging plane wave can be seen in Figure 9(a). The implemented RCS reduced frequency bandwidth is from 8

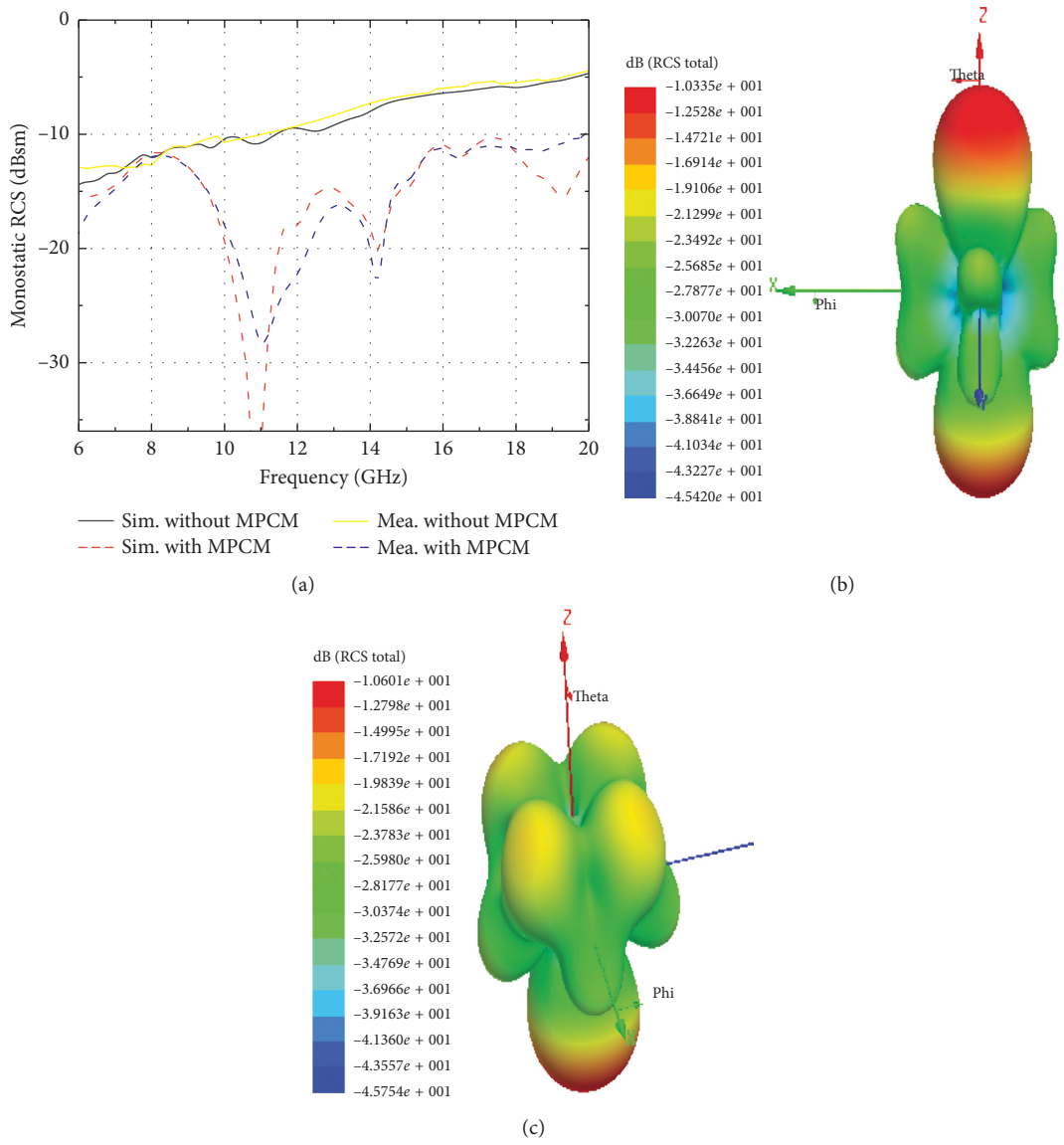

Figure 9: (a) Simulated and measured RCS of both antennas as a function of frequency for normal-impinging plane wave with x-polarization; 3D bistatic scattered field at 10 GHz under normal incidence for (b) antenna with CPCM and (c) antenna without CPCM.

to 20 GHz, and the RCS reduced band is consistent with the frequency band for PCR values greater than 0.7. In addition, the maximum RCS reduction value is at least 14 dB. Since the MPCM structure is symmetrical, the same effect is produced by a normal-impinging plane wave with y-polarization. Some differences can be observed between the simulation and the measurement; this occurs primarily because of tolerance during fabrication, measurement deviations, and environmental factors, all affecting the measured RCS results.

4. Conclusions

In this paper, a novel antenna is proposed. It features a broadband CP, high gain, and low RCS using MPCM. The RCS range is between 8 and 20 GHz and is lower than the reference antenna. Furthermore, the gain is increased in the operating bandwidth and the AR bandwidth is also broadened. The simulated and measured results show that there is an improvement in the scattering and radiation characteristics of the MPCM antenna. Therefore, the design presented in this research provides a new approach for implementing broadband CP, high-gain, and low-RCS antennas. This has potential for use in several applications, most notably in stealth platforms.

Data Availability

The data used to support the findings of this study are included within the article.

Conflicts of Interest

The authors declare that there are no conflicts of interest regarding the publication of this paper.

Acknowledgments

This research was partially supported by the Major Project of Provincial Natural Science Research of the University of Anhui Province of China (Grant nos. KJ2018ZD046 and 2017sxzx40), the Science and Technology Project of Anhui Province (Grant no. 1708085QF150), and the National Natural Science Foundation of China (Grant nos. 61801163 and 61871001).

References

[1] Y. Liu, K. Li, Y. Jia, Y. Hao, S. Gong, and Y. J. Guo, "Wideband RCS reduction of a slot array antenna using polarization conversion metasurfaces," *IEEE Transactions on Antennas and Propagation*, vol. 64, no. 1, pp. 326–331, 2016.

[2] L. Zhang and T. Dong, "Low RCS and high-gain CP microstrip antenna using SA-MS," *Electronics Letters*, vol. 53, no. 6, pp. 375-376, 2017.

[3] O. Altintas, E. Unal, O. Akgol, M. Karaaslan, F. Karadag, and C. Sabah, "Design of a wide band metasurface as a linear to circular polarization converter," *Modern Physics Letters B*, vol. 31, no. 30, article 1750274, 2017.

[4] O. Akgol, E. Unal, O. Altintas, M. Karaaslan, F. Karadag, and C. Sabah, "Design of metasurface polarization converter from linearly polarized signal to circularly polarized signal," *Optik*, vol. 161, pp. 12–19, 2018.

[5] O. Akgol, O. Altintas, E. Unal, M. Karaaslan, and F. Karadag, "Linear to left- and right-hand circular polarization conversion by using a metasurface structure," *International Journal of Microwave and Wireless Technologies*, vol. 10, no. 1, pp. 133–138, 2018.

[6] W. Pan, C. Huang, P. Chen, X. Ma, C. Hu, and X. Luo, "A low-RCS and high-gain partially reflecting surface antenna," *IEEE Transactions on Antennas and Propagation*, vol. 62, no. 2, pp. 945–949, 2014.

[7] C. Huang, W. Pan, X. Ma, and X. Luo, "A frequency reconfigurable directive antenna with wideband low-RCS property," *IEEE Transactions on Antennas and Propagation*, vol. 64, no. 3, pp. 1173–1178, 2016.

[8] Y.-j. Zheng, J. Gao, X.-y. Cao, S.-j. Li, and W.-q. Li, "Wideband RCS reduction and gain enhancement microstrip antenna using chessboard configuration superstrate," *Microwave and Optical Technology Letters*, vol. 57, no. 7, pp. 1738–1741, 2015.

[9] J. Hu, G. Q. Luo, and Z.-C. Hao, "A wideband quad-polarization reconfigurable metasurface antenna," *IEEE Access*, vol. 6, pp. 6130–6137, 2018.

[10] K. Li, Y. Liu, Y. Jia, and Y. J. Guo, "A circularly polarized high-gain antenna with low RCS over a wideband using chessboard polarization conversion metasurfaces," *IEEE Transactions on Antennas and Propagation*, vol. 65, no. 8, pp. 4289–4292, 2017.

[11] Y. Zhao, X. Cao, J. Gao, L. Xu, X. Liu, and L. Cong, "Broadband low-RCS circularly polarized array using metasurface-based element," *IEEE Antennas and Wireless Propagation Letters*, vol. 16, pp. 1836–1839, 2017.

[12] J. Han, X. Cao, J. Gao et al., "Broadband radar cross section reduction using dual-circular polarization diffusion metasurface," *IEEE Antennas and Wireless Propagation Letters*, vol. 17, no. 6, pp. 969–973, 2018.

[13] Y. Zhao, X. Cao, J. Gao, X. Yao, and X. Liu, "A low-RCS and high-gain slot antenna using broadband metasurface," *IEEE Antennas and Wireless Propagation Letters*, vol. 15, pp. 290–293, 2016.

[14] J. Wu, Z. Zhang, X. Ren, Z. Huang, and X. Wu, "A broadband electronically mode-reconfigurable orbital angular momentum metasurface antenna," *IEEE Antennas and Wireless Propagation Letters*, vol. 18, no. 7, pp. 1482–1486, 2019.

[15] H. Evans, P. Gale, B. Aljibouri, E. G. Lim, E. Korolkeiwicz, and A. Sambell, "Application of simulated annealing to design of serial feed sequentially rotated 2 X 2 antenna array," *Electronics Letters*, vol. 36, no. 24, pp. 1987-1988, 2000.

[16] K. K. Pang, H. Y. Lo, K. W. Leung, K. M. Luk, and E. K. N. Yung, "Circularly polarized dielectric resonator antenna subarrays," *Microwave and Optical Technology Letters*, vol. 27, no. 6, pp. 377–379, 2000.

[17] H. L. Zhu, S. W. Cheung, X. H. Liu, and T. I. Yuk, "Design of polarization reconfigurable antenna using metasurface," *IEEE Transactions on Antennas and Propagation*, vol. 62, no. 6, pp. 2891–2898, 2014.

[18] C. L. Holloway, E. F. Kuester, J. A. Gordon, J. O'Hara, J. Booth, and D. R. Smith, "An overview of the theory and applications of metasurfaces:The two-dimensional equivalents of metamaterials," *IEEE Antennas and Propagation Magazine*, vol. 54, no. 2, pp. 10–35, 2012.

[19] W. Liu, Z. N. Chen, and X. Qing, "Metamaterial-based low-profile broadband aperture-coupled grid-slotted patch antenna," *IEEE Transactions on Antennas and Propagation*, vol. 63, no. 7, pp. 3325–3329, 2015.